Atmos. Chem. Phys. Discuss., 11, 30627–30663, 2011
www.atmos-chem-phys-discuss.net/11/30627/2011/
doi:10.5194/acpd-11-30627-2011

Atmospheric Chemistry and Physics Discussions

The isotopic record of Northern Hemisphere atmospheric carbon monoxide since 1950, implications for the CO budget

Z. Wang[1], J. Chappellaz[2], P. Martinerie[2], K. Park[1,*], V. Petrenko[3,], E. Witrant[4], T. Blunier[5], C. A. M. Brenninkmeijer[6], and J. E. Mak[1]**

[1]Institute for Terrestrial and Planetary Atmospheres/School of Marine and Atmospheric Sciences, State University of New York at Stony Brook, Stony Brook, NY 11794, USA
[2]UJF – Grenoble 1/CNRS, Laboratoire de Glaciologie et Géophysique de l'Environnement (LGGE) UMR 5183, Grenoble, 38041, France
[3]Institute of Arctic and Alpine Research, University of Colorado, Boulder, CO 80309, USA
[4]Grenoble Image Parole Signal Automatique (GIPSA-lab), Université Joseph Fourier/CNRS, BP 46, 38 402 Saint Martin d'Hères, France
[5]Centre for Ice and Climate, Niels Bohr Institute, University of Copenhagen, Juliane Maries vej 30, 2100 Copenhagen Ø, Denmark
[6]Max Planck Institute for Chemistry, 55128 Mainz, Germany

* now at: Division of Polar Climate Research, Korea Polar Research Institute, Incheon, South Korea
** now at: Department of Earth and Environmental Sciences, University of Rochester, Rochester, NY, USA

Received: 24 October 2011 – Accepted: 28 October 2011 – Published: 15 November 2011

Correspondence to: Z. Wang (zhihui.wang@stonybrook.edu)

Published by Copernicus Publications on behalf of the European Geosciences Union.

Abstract

We present a 60-yr record of atmospheric CO concentration and stable isotopic ratios at high northern latitude based on firn air samples collected in the frame of the North Greenland Eemian Ice Drilling (NEEM) project. Concentration, δ^{13}C, and δ^{18}O of CO from trapped gases in the firn were measured by gas chromatography coupled with isotope ratio mass spectrometry (gc-IRMS). Using models of trace gas transport in firn, the long-term trend of atmospheric CO and its stable isotopic composition at high northern latitudes since the 1950s were reconstructed. Our best firn air scenarios suggest that δ^{13}C decreased slightly from −25.8 ‰ in 1950 to −26.4 ‰ in 2000, then dropped to −27.2 ‰ in 2008. δ^{18}O decreased more regularly from 9.8 ‰ in 1950 to 7.1 ‰ in 2008. The best firn air scenarios also suggest that CO concentration increased gradually from 1950 and peaked likely in the late-1970s, followed by a gradual decrease by present day (Petrenko et al., 2011). An isotope mass balance model is applied to quantify the temporal evolution of CO source partitioning able to explain the combined mixing ratio and isotopic ratio changes. It suggests that a slight increase followed by a large reduction in CO derived from fossil fuel combustion occurred since 1950. The increase of CO concentration from 1950 to the mid-1970s is the result of a combined increase of multiple sources. The reduction of CO emission from fossil fuel combustion after the mid-1970s is the most plausible mechanism for the drop of CO concentration during this time. The mitigation policy for CO emission from vehicle exhaust such as application of catalytic converters and the growth of diesel engine vehicles market share are the main expected reasons for the CO source strength change from fossil fuel combustion.

1 Introduction

The importance and interest for reconstructing past atmospheric CO arises from its significant role on the chemistry of the troposphere, since CO is a major sink for hydroxyl

ACPD
11, 30627–30663, 2011

radical (OH). Thus its abundance affects the lifetimes of reactive greenhouse gases and ozone depleting gases. In addition to its significance for OH, oxidation of CO by OH provides a source (high NO_x) or a sink (low NO_x) for ozone, which is a major contributor to ground level photochemical smog under high NO_x conditions (Levy, 1971; Logan et al., 1981). The major sources of atmospheric CO in today's atmosphere include oxidation of methane (CH_4) and non-methane hydrocarbons (NMHC), biomass burning, fossil fuel and biofuel combustion (Duncan et al., 2007; Seiler, 1974). In addition to a complex mixture of sources, atmospheric CO has a relatively short global averaged lifetime (Weinstock, 1969), resulting in large temporal and spatial variations and adding difficulties in determining the global CO budget (Brenninkmeijer and Rockmann, 1997). Certain sources produce atmospheric CO with distinct ratios of $^{13}C/^{12}C$ and $^{18}O/^{16}O$ (Stevens et al., 1972; Stevens and Wagner, 1989; Brenninkmeijer, 1993), hence isotopic information can help to determine the various sources and their relative magnitudes (Mak et al., 2003; Mak and Kra, 1999; Mak and Brenninkmeijer, 1998; Rockmann et al., 2002; Manning et al., 1997). Bergamaschi et al. reported that introducing isotope data in source optimization provides relatively well constrained source strengths of CO (Bergamaschi et al., 2000a,b). However, only few observations exist from which the relative source strengths in past atmospheres can be estimated. Polar ice core analyses have provided hints about the evolution of CO from its concentration (Ferretti et al., 2005; Haan et al., 1996; Haan and Raynaud, 1998; Wang et al., 2010) and isotopic ratios (Wang et al., 2010) over the last few centuries. They notably revealed the importance of biomass burning changes in the Southern Hemisphere in controlling past CO in Antarctica (Wang et al., 2010). A recent study based on firn air analyses has provided a reconstruction of atmospheric CO from Berkner Island, Antarctica, roughly covering the last decades, which is important for understanding the past CO budget in the Southern Hemisphere (Assonov et al., 2007). However, there is limited information about the 20th century CO evolution in the Northern Hemisphere. The only available firn air CO measurements from the Northern Hemisphere were performed on firn air collected from the summit of Devon Island Ice Cap, Nunavut, Canada

ACPD
11, 30627–30663, 2011

(75°20′ N; 82°08′ W; 1929 m a.s.l.) in April 1998 (Clark et al., 2007). However, they showed the existence of in-situ CO production with depth, likely related to the relatively high temperature of this site, associated with systematic summer melting and thick melt layers in the firn column, as well as relatively high levels of impurities in Devon Island ice.

Greenland ice core records have shown that CO concentration at high northern latitudes increased from ~90 ppbv to ~110 ppbv between 1800 and 1950 (Haan et al., 1996), which is believed to result from rising anthropogenic emissions such as fossil fuel combustion (Marland et al., 2008). Today's annual mean CO concentration over Summit, Greenland (72.58° N; 38.48° W; 3238 m a.s.l.) is around 120 ppbv based on flask measurements by National Oceanic and Atmospheric Administration Global Monitoring Division (NOAA/GMD) (Novelli and Masarie, 2010). Therefore comparing ice core and direct atmospheric CO measurements suggests that significant variations of CO concentration and concurrent CO budget occurred over the last 60 yr. However, the observations of atmospheric CO before 1988 were limited and the CO data earlier than 1980 is very sparse. The only available atmospheric CO concentration for 1950–1951 was deduced indirectly from infrared total column amount measurements at the Jungfrau Scientific Station in the Swiss Alps (Rinsland and Levine, 1985). The field measurements of atmospheric CO started in the early 1970s (Seiler and Junge, 1970; Seiler, 1974; Heidt et al., 1980) and systematic global monitoring of atmospheric CO by National Oceanic and Atmospheric Administration Global Monitoring & Diagnostics Laboratory (NOAA/CMDL) started in the late 1980s (Novelli et al., 1992, 1994). An increasing trend of atmospheric CO at Cape Meares, Oregon (45° N; 125° W) was first recognized in 1979–1982 (Khalil and Rasmussen, 1984), and a decrease in global CO concentration was observed in early 1990s (Khalil and Rasmussen, 1994; Novelli et al., 1994).

In this study, we present a record of CO concentration and stable isotopic ratios at high northern latitudes since about 1950, based on measurements of firn air samples collected at the NEEM ice core drilling site in Greenland. Due to signal smoothing by

ACPD
11, 30627–30663, 2011

diffusion of gases in firn air (Schwander and Stauffer, 1984), firn air measurements do not provide discretely resolved time evolutions of trace gas concentrations and isotopic ratios. Models of trace gas transport in firn are thus used to derive this reconstruction from the observed firn air profile. The evolving CO budget over the last 50 yr at high northern latitudes is then calculated based on measurement of CO concentration, $\delta^{13}C$, $\delta^{18}O$ and an isotope mass balance model (Wang et al., 2010; Mak and Kra, 1999).

2 Experimental procedures

Within the framework of the international project NEEM, 18 firn air samples from surface to 75.9 m of depth were obtained close to the NEEM deep drilling site (77.445° N; 51.066 ° W; 2484 m a.s.l.) in July 2008. Details of the NEEM 2008 firn air campaign have been described recently (Buizert et al., 2011). The NEEM firn air samples used here were collected from the 2008 EU borehole (Buizert et al., 2011) in 3 l Silco cans (Restek Inc.) at a pressure of 2.8 bar. Before being filled, the Silcocans already included polar firn air from previous expeditions, at pressure above ambient. The firn air was dried through a $Mg(ClO_4)_2$ trap put on-line between the pumping unit and the Silcocan. The filling procedure included evacuation of the Silcocan first, then two times filling to 1 atm above ambient followed by evacuation, and lastly filling to 2.8 bar. The surface sample was collected on 16 July 2008 at 10:00 p.m. local time. The air samples were then analyzed with an established protocol (Wang and Mak, 2010) at Stony Brook University in November/December 2008, 5 to 6 months after collection. Concentration and isotopic ratios ($\delta^{13}C$ and $\delta^{18}O$) were determined based on on-line cryogenic vacuum extraction followed by continuous-flow isotope ratio mass spectrometry (CF-IRMS) (Wang and Mak, 2010). 100 ml sample (STP) was processed at a flow rate of 50 ml min^{-1} for each run and 3 to 12 replicates were conducted for each sample. Calibration gas (CO mixing ratio 141 ppbv; $\delta^{13}C = -45.56$ ‰ VPDB; $\delta^{18}O = -1.94$ ‰ VSMOW) (Wang and Mak, 2010) was processed frequently between firn air samples,

ACPD
11, 30627–30663, 2011

and the measurement results are shown in Fig. 1. Analytical precision of 3 ppbv ($\pm 1\sigma$) for CO concentration, 0.3 ‰ ($\pm 1\sigma$) for $\delta^{13}C$ and 0.8 ‰ ($\pm 1\sigma$) for $\delta^{18}O$ was obtained for 100 ml firn air sample (STP).

Firn air samples were also collected from the same borehole (EU Borehole) in glass flasks and analyzed for CO concentration at CSIRO, Australia, University of Heidelberg, Germany, as well as at NOAA/CMDL, USA, allowing for inter-laboratory comparison. In addition, the 2008 US borehole (Buizert et al., 2011) was sampled and measured for CO concentration at NOAA/CMDL and the University of Heidelberg (Petrenko et al., 2011).

3 Results

CO concentration and isotope profiles from NEEM firn air are shown in Fig. 2. Details on discussions of CO concentration will be presented in a separate paper (Petrenko et al., 2011) and CO concentration here is mainly used to evaluate our CO data with respect to others. Good agreement of CO concentration trend was observed among four independent labs, although there are differences in absolute values, most probably reflecting different in calibration scales (see Petrenko et al., 2011, for further discussion). The concentration profiles show that, on the Stony Brook scale, [CO] increases from 85 ppbv to 140 ppbv between the surface and 20 m of depth, followed by a relatively constant value of around 130 ppbv to a depth of 60 m. The first feature results from the seasonal variation of atmospheric CO concentrations, which ranged from, e.g., around 160 ppbv in February 2008 to around 90 ppbv in August 2008 to in Summit, Greenland (72.58° N; 38.48° W; 3238 m a.s.l.) (Novelli and Masarie, 2010). The surface observation on 16 July 2008, thus lies on the downward trend of the seasonal cycle, whereas below about 35 m depth, the observed firn air CO concentration already reflects an average atmospheric concentration over at least one year. A gradual increase of CO concentration is then observed from 60 m to 70 m, with measured peak value of around 155 ppbv at 70 m, followed by a gradual decrease down to the bottom of the firn.

ACPD
11, 30627–30663, 2011

CO concentration peak at 70 m in NEEM firn layer is reproduced in deep NGRIP (North Greenland Ice Core Project) firn, as well as deep firn at Summit, Greenland with similar peak value (Petrenko et al., 2011), indicating CO is well preserved in NEEM firn and that in-situ CO production affecting the firn air composition is unlikely at Greenland sites without summer melting. The measured mixing ratio profiles for other trace gases such as SF_6 also confirm that most NEEM samples are free of contamination with ambient air and contamination in deepest samples is minimal (Buizert et al., 2011).

As for the CO isotopes, a seasonal imprint of both $\delta^{13}C$ and $\delta^{18}O$ in the first 0–50 m is observed in NEEM firn (Fig. 2 and Sect. 4.2). $\delta^{13}C$ of atmospheric CO at Alert was −29 ‰ in September 1997 and −24 ‰ in May 1998, where $\delta^{18}O$ ranged from −2 ‰ in August 1997 to 10 ‰ in February 1998 (Rockmann et al., 2002). Our isotopic ratio data then exhibit more enriched values for $\delta^{13}C$ below 50 m and for $\delta^{18}O$ below 60 m. As the mass difference between the ^{13}CO–^{12}CO ($C^{18}O$–$C^{16}O$) equals to 1 (2), the enrichment with depth of ^{13}CO ($C^{18}O$) with respect to the ^{12}CO ($C^{16}O$) due to gravitational fractionation must be similar (twice) as gravitational enrichment of ^{15}N–^{14}N versus ^{14}N–^{14}N of molecular nitrogen. In the NEEM firn, $\delta^{15}N$ of N_2 amounts to 0.3 ‰ in the deepest air samples (Buizert et al., 2011). Thus gravitational enrichment (0.3 ‰ for $\delta^{13}C$ and 0.6 ‰ for $\delta^{18}O$) cannot account alone for the observed enrichment of CO heavier isotopologues. This enrichment has to reflect diffusion gradients in the NEEM firn and potential atmospheric changes of the CO isotopic ratios over the last several decades.

4 LGGE-GIPSA models of gas transport in firn

4.1 Model description

A 1-D inverse model initially developed by Rommelaere et al. (1997) and recently extended to isotopes was used to reconstruct the atmospheric trends of CO isotopes. The full procedure involves a suite of three models of gas transport in firn. A forward

ACPD
11, 30627–30663, 2011

model provides the physical basis of all models and simulates a concentration profile in firn using an atmospheric trend scenario as input. It needs to be constrained by a depth profile of effective diffusivity in firn which is calculated by a new multi-gas constrained optimization model. The LGGE-GIPSA forward and diffusivity optimization models (Witrant et al., 2011) showed very good performances in a model comparison study based on the two NEEM 2008 firn air pumping operations (Buizert et al., 2011). Alternatively, using a Dirac function as input, the forward model calculates a trace gas age distribution (or Green function) which defines the response of the firn to a trace gas change at the surface (Rommelaere et al., 1997).

Once the forward model has been properly constrained for a given firn air pumping site, the second step is to calculate the atmospheric trend scenario. The above Green function and the target gas firn air concentrations with uncertainties are then used as input to the inverse scenario diffusion model, in order to produce the calculated atmospheric trend. An infinite number of solutions can fit the data satisfactorily, thus a regularization term aiming at selecting the simplest solution is used (Rommelaere et al., 1997). Isotopic records in firn are expressed as the deviation from a reference of a concentration ratio between the major isotopologue and the target minor isotopologue (δ unit). This unit is not mass-conservative and thus cannot be directly used in most modeling studies. The variations with depth of isotopic ratios in firn can be due to variations in the major isotopologue concentrations, the minor isotopologue concentrations, or both. Moreover, molecular diffusion coefficients are mass dependent (see e.g., Supplementary material in Buizert et al., 2011), thus trace gas transport in firn induces an isotopic fractionation. The scenario reconstruction method used here is based on separating the effects of the major and minor isotopologues on their concentration ratio. The effect of the major isotopologue is first evaluated by using its atmospheric time trend as input to the forward model. A second forward model simulation calculates minor isotopologue concentrations in firn resulting from the latter scenario and a constant isotopic ratio in the atmosphere. Then the isotopic ratios measured in firn are corrected from this major isotopologue effect and the resulting values are inverted

ACPD
11, 30627–30663, 2011

assuming a constant atmospheric concentration of the major isotopologue. The final evaluation of the reconstructed atmospheric isotopic ratio is done by running again both the major and minor isotopologue trends in the forward model (the latter is calculated with regular δ to minor isotope concentration conversion using the former) in order to check the consistency of the resulting isotopic ratios in firn with the measured values.

In the case of CO isotopes, a data based CO concentration trend at Barrow, Alaska (71.32° N 156.61° W 11 m a.s.l.) is available only since 1988 (Novelli and Masarie, 2010), thus an inverse model CO concentration trend (Petrenko et al., 2011) is used in the reconstruction of atmospheric isotopic ratios for CO isotopes. Sensitivity tests were performed in order to evaluate the effect of the uncertainty of the past CO trend on isotope reconstructions (see Sect. 4.4).

4.2 Impact of seasonal cycles on CO firn signals

Atmospheric CO and its stable isotopic ratios undergo strong seasonal variations (Mak et al., 2003; Manning et al., 1997; Rockmann et al., 2002). In this section, we aim at understanding how and until which depth firn results are affected by seasonality. The regularization term used in the inverse model for long-term atmospheric trend reconstruction requires the use of a small second derivative of the scenario. Thus the inverse model scenarios cannot capture seasonal changes. As a consequence, the reconstruction of a long term atmospheric trend requires us to discard the firn data strongly influenced by seasonality and/or correct the data from the effect of seasonality.

Mean atmospheric seasonal cycles were estimated from atmospheric records of CO, δ^{13}C, and δ^{18}O of CO in Iceland (Wang et al., 2011). Using the forward model, the effect of seasonality on firn records is estimated on Fig. 3 for our target isotopic ratios as the difference between concentrations in firn resulting from a constant atmospheric scenario, and from a constant mean annual atmospheric scenario with a perpetual mean seasonality. The difference between both scenarios indicates that CO isotopic ratios in firn can be seasonally influenced down to 50 m depth, and that most of the observed δ^{13}C and δ^{18}O variations in the upper ~ 40 m of the NEEM firn can be explained

ACPD
11, 30627–30663, 2011

by the effect of seasonality (Fig. 3). However the amplitude of the seasonal effect is small between 30 and 40 m depth (less than 0.1 ‰). Between 20 to 30 m, sub-monthly time scale events in the atmosphere still potentially have a significant influence.

For the purpose of inverse modelling, our estimate of the seasonal effect was considered as acceptable when the corrected values fall within the mean uncertainty of the measured values. Thus the uppermost 3 data points for δ^{13}C and 2 data points for δ^{18}O of CO were discarded. Seasonally corrected data were used at lower depths.

4.3 Atmospheric trend reconstructions for δ^{13}C and δ^{18}O of CO

Best estimate atmospheric trends of CO concentration taken from (Petrenko et al., 2011), δ^{13}C and δ^{18}O of CO are shown in Fig. 4. CO concentration trend will be discussed in Petrenko et al. (2011). We focus on CO isotopes here. Atmospheric trends of δ^{13}C and δ^{18}O are required to explain the signal trends below 40 m of depth but show small amplitude variations. The bell shape of the firn signals around 65 m depth is mainly explained by the effect of the major isotopologue which peaks at similar depth in the firn. The root mean square deviation of the model results with respect to firn data ($RMSD_{mod}$) is 0.27 ‰ for δ^{13}C and 0.65 ‰ for δ^{18}O. These numbers are comparable to the experimental uncertainties. Varying the weight of the regularization term (e.g. the imposed smoothness of the scenario) has more influence on δ^{13}C than δ^{18}O (Fig. 5). The optimal solution for δ^{18}O is nearly a linear trend with time. With a less regular scenario, the model essentially tries to reduce the data-model discrepancy with the data point at 70 m depth. However, due to the gas age overlaps with the neighboring data points at 68 and 72 m depth, an exact fit of the 70 m depth data would require a very strong and unrealistic variation in the atmospheric scenario. The variations of $RMSD_{mod}$ when varying the weight of the regularization term by five orders of magnitudes are small: 0.63–0.70 ‰. $RMSD_{mod}$ varies more strongly for δ^{13}C of CO: 0.19–0.31 ‰, in relation with a less stable behavior of the solution (Fig. 5). In the firn, a less regular scenario for δ^{13}C produces a steeper slope in the upper firn (0–60 m). The higher/lower atmospheric values with respect to the optimal scenario

ACPD
11, 30627–30663, 2011

can be related to higher/lower values in different depth ranges in firn which result in the oscillating behavior of the scenario (the increasing values below 65 m are associated with an atmospheric increase before 1952). The decreasing atmospheric trend in $\delta^{13}C$ in 2004–2008 is overall consistent with atmospheric data in Iceland (Wang et al., 2011) but it should be reminded that at such short time scale, the model may not discriminate between the multi-annual trend and sub-annual events such as seasons with strong biomass burning events.

4.4 Effect of CO past trend on isotope reconstructions

Isotopic ratios in firn are sensitive to variations of both the major and minor isotope (see Sect. 4.1). Here we test the effect of uncertainties in the past CO trend on isotopic ratios. Eleven CO scenarios were built, aiming at covering the range of uncertainties (see Supplement Fig. S1). Five of them use NEEM EU hole only CO data and smoothing factors differing by five orders of magnitude, the other use different ways of averaging single or multi-site simulations and connecting them to the ice core data (Haan et al., 1996) (with or without rescaling). Supplement Fig. S1 shows the impact on $\delta^{13}C$ and $\delta^{18}O$ of using these different CO scenarios to reconstruct atmospheric isotopic trends. The induced differences in both the atmospheric trends and the matching of firn data fall well within uncertainties illustrated in Figs. 4 and 5. This indicates that the impact on $\delta^{13}C$ and $\delta^{18}O$ of using these different CO scenarios to reconstruct atmospheric isotopic trends is very small.

4.5 Sensitivity to the deepest measurement for $\delta^{13}C$ of CO

Trace gas concentrations in deep firn are affected by air removal from the firn by trapping in bubbles. They also undergo the longest age mixing. As a consequence, they do not constrain well the atmospheric trend at the times corresponding to their age distribution. The inverse model being only partially constrained, the fit of the deepest firn data is dependent on scenario values at longer time scales than its significant length.

ACPD
11, 30627–30663, 2011

Supplement Fig. S2 illustrates the effect of not using the deepest measurement of $\delta^{13}C$ as a constraint for the inverse model. The results remain within error bars between 1940 and 2008 but lead to a somewhat different shape of the scenario for the whole period. Figure S2 suggests that the early trend in $\delta^{13}C$ (before ~1975) is influenced by the last data point.

5 Discussions

The variation of CO concentration as well as the shifts of both isotopic ratios since 1950 indicates significant variations in CO source strengths and/or a change in the CO loss rate. Isotopic ratios help us to distinguish between CO from different sources (Brenninkmeijer, 1993; Stevens et al., 1972; Stevens and Wagner, 1989). Notably $C^{18}O$ is a good tracer for distinguishing combustion-derived CO (e.g. fossil fuel combustion or biomass burning) from non-combustion derived CO (e.g. hydrocarbon oxidation) (Brenninkmeijer and Rockmann, 1997). ^{18}O enriched sources are fossil fuel combustion, biomass burning and biofuel (Stevens et al., 1972; Stevens and Wagner, 1989; Kato et al., 1999; Brenninkmeijer and Rockmann, 1997).

An isotope mass balance model is used to quantify the different source partitioning (Mak and Kra, 1999; Wang et al., 2010). The isotope mass balance model used in this study includes the following equations:

$$\sum_{i=1}^{7}[CO_i]=[CO] \quad (1)$$

$$\sum_{i=1}^{7}[CO_i]\times\delta^{18}O_i=[CO]\times\delta^{18}O \quad (2)$$

where i denotes a given CO source: fossil fuel combustion, methane oxidation, NMHC oxidation, biofuel burning, biomass burning, direct biogenic, and oceanic emission. $[CO_i]$ stands for CO concentration from each source and [CO] is the atmospheric CO

ACPD
11, 30627–30663, 2011

concentration derived from Greenland firn air measurements and diffusion model simulations (Petrenko et al., 2011). $\delta^{18}O_i$ is the $\delta^{18}O$ source signature at high northern latitude and $\delta^{18}O$ is the $\delta^{18}O$ of atmospheric CO from NEEM firn air measurements and diffusion model simulations in this study (Fig. 4). Both the best estimate of CO concentration and $\delta^{18}O$ values and envelope values from LGGE-GIPSA models simulation will be used to calculate the mean source partitioning and uncertainties.

The $\delta^{13}C$ data are not used in the mass balance calculation because $\delta^{13}C$ signatures for different Northern Hemisphere CO sources have much larger uncertainties. First, the $\delta^{13}C$ signature for biomass burning is largely uncertain since it is dependent on the burned C3/C4 plants ratio, which could vary temporally and will be hard to be determined. Second, $\delta^{13}C$ signatures for NMHC oxidation are also highly uncertain since different NMHC have different carbon isotopic signatures (Rudolph et al., 1997) and particularly the kinetic isotope effects for NMHC + OH cover a large range for different NMHCs (Iannone et al., 2003, 2009; Rudolph et al., 2000). Therefore, only $\delta^{18}O$ is used in the following mass balance calculation. A more detailed discussion of $\delta^{13}C$ data is provided in the Supplement.

Assuming steady state, which is reasonable since CO lifetime is much shorter than the decadal scale we are interested in, the contribution of methane to CO is only dependent on the abundance of methane. [CO] from methane oxidation at high northern latitude is calculated based on an atmospheric methane concentration trend (Buizert et al., 2011) and the following equation:

$$[CO]_{CH_4} = k_1/k_2 \times [CH_4] \quad (3)$$

where $[CO]_{CH_4}$ is the methane-derived [CO], k_1 is the rate constant of $CH_4 + OH$ reaction, k_2 is the rate constant of CO +OH reaction, and $[CH_4]$ is the methane concentration.

The $\delta^{18}O$ signatures for different sources and [CO] contributions from these sources in modern atmosphere at high northern latitude (Iceland: 63°15′ N 20°09′ W) have been calculated with MOZART-4 model simulations (Model for Ozone and Related Chemical Tracers, version 4) (Emmons et al., 2010; Park, 2010) (Table 1). Simulations on

ACPD
11, 30627–30663, 2011

other high northern latitudes such as Alert (78.5° N 11.5° W) and Spitsbergen (81.3° N 62.3° W) show very consistent results on CO contributions and $\delta^{18}O$. Variations of $\delta^{18}O$ source signatures over time are not taken into account since the mechanisms of CO derived from different sources such as fossil fuel combustion, biomass burning, NMHC/CH_4 oxidation etc. are assumed to be constant over the last 60 yr.

In the isotope mass balance model and in order to reduce the number of free parameters in the equation, biogenic and marine emissions since 1950 are fixed at today's values and their [CO] contributions are shown in Table 1. Marine CO emission is tiny (1 %) and it is dependent on the solar radiation (particularly UV irradiance) and dissolved organic matter (DOM) (Bauer et al., 1980; Conrad and Seiler, 1980). UV irradiance may have increased by 1.42 % since 1610 (Lean et al., 1995). Very large variation of global or hemispheric ocean DOM amount did not likely occur in a short period of time (e.g. 50 yr). A constant marine emission can thus be reasonably assumed. Direct biogenic emission accounts for 10 % and it is likely a result of direct photochemical transformation occurring inside the leaf (Tarr et al., 1995). We assume that biogenic emission is dependent on solar radiation and the amount of biomass (or roughly on vegetation area). Considering small changes of vegetation area from 10 different world regions in 1950–1992 (Pongratz et al., 2008), the biogenic emission of CO is assumed to be constant since 1950.

Biomass burning contribution is calculated based on simulated present-day value at Iceland 1997–2004 (Table 1) and biomass burning reconstructions for the past. It has been found that around 90 % of biomass burning-derived CO at high northern latitudes originates mainly from the Northern Hemisphere (NH) (Park, 2010). We use historical NH CO emission from biomass burning in 1950–2000 (Ito and Penner, 2005) and biomass burning CO contribution at Iceland in 1997–2004 from MOZART-4 simulation (Table 1; Park, 2010) to scale the biomass burning contribution at the NEEM site since 1950. An uncertainty of ± 50 % is considered in the scaling based on the uncertainty suggested in Ito and Penner (2005). The resulting CO contribution from biomass burning bears a ± 35 % uncertainty if we use historical global biomass burning CO emission

ACPD
11, 30627–30663, 2011

data instead of NH biomass burning CO emission data (Ito and Penner, 2005). The CO contributions from biomass burning calculated from other historical global biomass burning CO emission using model simulations (van Aardenne et al., 2001; Lamarque et al., 2010) and global wildfire simulations (Pechony and Shindell, 2010) (they assume that CO emission from biomass burning is proportional to the fire activity each year in 1950–2000) are within a ± 50 % envelope.

CO derived from biofuel emission at high northern latitudes originates mainly from the Northern Hemisphere (Park, 2010). Between 1950 and 2000, biofuel use in Asia and Africa grew rapidly and dominates the global biofuel use as a result of population growth in the developing countries (Fernandes et al., 2007). We thus use historical NH CO emission from biofuel burning in 1950–2000 (Ito and Penner, 2005) and biofuel burning CO contribution at Iceland in 1997–2004 from MOZART-4 simulation (Table 1) to scale the biofuel burning contribution at the NEEM site since 1950. An uncertainty of ± 50 % is considered in the scaling based on the uncertainty suggested in Ito and Penner (2005). Even if we use historical global biofuel burning CO emission data instead of NH biofuel burning CO emission data (Ito and Penner, 2005), the results of CO contribution from biofuel burning remain within a ± 50 % envelope. Results based on other historical global biofuel burning CO emission model simulations (van Aardenne et al., 2001) are also within the ± 50 % envelope. The historical CO emissions from NH biomass and biofuel burning and relevant CO contribution by scaling are shown in Fig. 6. The biomass and biofuel inventory during 1997–2000 used in MOZART-4 simulation is within the uncertainty of those in historical reconstructions (Ito and Penner, 2005). The 1997–2000 CO contributions calculated by MOZART-4 simulation also agree well with those from the scaling method decribed above, except for year 1998 which is affected by large wildfires.

The two remaining variables are fossil fuel combustion and NMHC oxidation, which can be evaluated from the above equations based on the CO reconstruction data from LGGE-GIPSA models (Fig. 4).

ACPD
11, 30627–30663, 2011

So far, we have assumed that the observations were driven by variations in CO source strengths. It is possible, however, that the removal rate of CO by OH could have changed. Previous studies showed that interannual variation of atmospheric OH is less than 10 % since the late 1970s (Prinn et al., 2005; Bousquet et al., 2005). This 10 % variation causes δ^{18}O of CO changes of only 0.5 ‰ based on MOZART-4 simulation, which is lower than our analytical uncertainty. A recent study suggests that the interannual variability of global [OH] was less than 5 % during 1985–2008 (Montzka et al., 2011). There is no [OH] record available before the end of 1970s. Therefore, we assume CO removal by OH has been constant over the past 50 yr.

The temporal evolution of CO partitioning between fossil fuel combustion and NMHC oxidation since 1950 calculated by the isotope mass balance model (Wang et al., 2010) is shown in Fig. 7. It clearly suggests a dominant control from fossil fuel combustion variation at high northern latitude since 1950 on the δ^{18}O trend in Fig. 4. The first feature along time is that CO contribution from methane oxidation has continuously increased since 1950, which mainly causes a decrease of δ^{18}O, since methane oxidation source is depleted in ^{18}O. We also find that no significant change in NMHC oxidation has occurred since 1950. However, large variations of CO emissions from fossil fuel combustion are suggested to have occurred since 1950. CO contribution from fossil fuel combustion increased slightly from 1950 to the mid-1970s, and started to decrease since then, and decreased 30 % from the mid-1970s to 2000. CO from fossil fuel combustion was as large as 59 % of all CO sources at high northern latitudes in 1950, which is much larger than that for present day (32 % in Table 1). The increase of [CO] from 1950 to the mid-1970s is thus the result of a combined increase of all sources except for the two fixed sources. The decrease of δ^{18}O during this time is mainly caused by the increase of CO contribution from methane oxidation. The combined decrease of [CO] and its δ^{18}O after the mid-1970s requires the decrease of CO contribution from fossil fuel combustion during this time.

MOZART-4 simulation shows that CO at high northern latitude originates from three major regions: North America, Western Europe, and Northern Asia (Park, 2010). The

ACPD
11, 30627–30663, 2011

historical fossil fuel CO_2 emissions in 1950–2006 for these three regions are shown in Fig. 8. CO_2 emissions from fossil fuel combustion increased from 1950 to the mid-1970s, implying an increase of CO emissions from fossil fuel combustion during this time (Fig. 7). On the other hand, the decrease of CO contribution after the mid-1970s from our calculation (Fig. 7c) goes opposite with a net CO_2 emission increase of ~ 20 % between the mid-1970s and 2000.

We propose that the reduction of CO from fossil fuel combustion after the mid-1970s reflects the implementation of catalytic converters in thermal-engine vehicles in North America during this time. The catalytic converter was invented and was applied in vehicles since late 1970s largely in the United States and Canada (Kummer, 1980; Young and Finlayson, 1976). Catalytic converters effectively reduce the CO emission from vehicle exhaust (Tsunogai et al., 2003) based on the oxidation reaction $2CO + O_2 \rightarrow CO_2$. CO emission from fossil fuel combustion would thus have dropped since the mid-1970s, counteracting the CO growth due to the concomitant CH_4 increase. It would explain at least partly the [CO] peak in the late 1970s (Petrenko et al., 2011) and the decrease of its $\delta^{18}O$ (Fig. 4).

Catalytic converters were introduced in Europe in 1975 and became mandatory in 1993. As a result, the CO emissions from fossil fuel combustion in Europe likely decreased only in the 1990s, which could cause the drop of CO from fossil fuel combustion during this time. Moreover, growth of market share for diesel engine vehicles, improvements in the automobile technologies including three-way oxidation/reduction catalytic converters, electronic ignition, fuel injection, and engine computer control in the period 1990-present have possibly resulted in further reductions in vehicle CO emissions.

Lead in gasoline can spoil the catalytic converter by forming a coating on the surface of the catalyst and disable the converter effectively. Vehicle manufacturers thus required the oil companies to remove lead from gasoline and substitute it with other chemical compounds to maintain the octane number (methyl tert-butyl ether (MTBE) in the USA, or higher concentration of benzene, toluene, ethylbenzene and xylenes

ACPD
11, 30627–30663, 2011

(BTEX) in Europe). The temporal variations of lead concentration in the Northern Hemisphere should thus reflect the timeline of the application of catalytic converters. The mandated phase-out of leaded gasoline preceded the application of catalytic converters, suggesting the decrease of Pb emissions preceded the decrease of CO emissions from fossil fuel combustion. Resulting from widespread use of leaded gasoline, Greenland ice core Pb concentration increased sharply from the 1950s and generally remained high until 1970 (Fig. 9). With passage of the US Clean Air Act and similar legislation in other countries (McConnell et al., 2002; McConnell and Edwards, 2008), the Pb concentration started to drop after 1970. Most of the decline in Pb concentration since the early 1970s came from the mandated phase-out of leaded gasoline, which allowed the usage of catalytic converters and reduced the on-road vehicle emissions significantly (McConnell et al., 2002). The US on-road vehicle Pb emissions dropped more than 99 % from 156 003 metric tons in 1970 to 17 metric tons in 1998 (EPA, 2000). Figure 9 indicates that the drop of Pb emissions from vehicles was followed by that of CO emissions from fossil fuel combustion. This is consistent with the expectation and supporting our conclusion that catalytic converters largely decrease the on-road vehicle CO emissions affecting CO concentrations over Greenland.

Previous model simulations based on energy consumption data and emission factors (Lamarque et al., 2010; van Aardenne et al., 2001) suggested that global anthropogenic emissions of CO had been steadily increasing from 1950 to 1990. One of the main anthropogenic sources of atmospheric CO is emissions from fossil fuel combustion (Duncan et al., 2007), most of which is taking place in Northern Hemisphere (Petron et al., 2004). However, our results combining CO concentration evolution with those of its δ^{18}O isotopic signature suggest that CO emission from fossil fuel combustion has been decreasing since the late-1970s in the Northern Hemisphere. The continuous increase of CO emissions from biomass/biofuel burning and fossil fuel combustion in model simulations (Lamarque et al., 2010; van Aardenne et al., 2001) could not explain the observed atmospheric trend of CO concentration (Petrenko et al., 2011) and of its δ^{18}O (Fig. 4). In contrast, our calculated temporal evolution of CO

ACPD
11, 30627–30663, 2011

contribution from fossil fuel combustion more likely explains both signals as fossil fuel combustion is the biggest source and the most ^{18}O enriched CO source at high northern latitudes. A very recent study has assessed several different inventories of global and regional anthropogenic and biomass burning emissions for the 1980–2010 period and large discrepancies of CO emissions for both global and regional are identified (Granier et al., 2011). Our conclusion thus raises unanswered questions on the reason of the inconsistency between the previous model simulations and the present calculation of fossil fuel combustion CO emissions in the Northern Hemisphere. This could have consequences for correctly estimating the radiative forcing of tropospheric ozone in the past as it directly depends on CO emission scenarios.

6 Conclusions

In this study, we present the first record of isotopic ratios of carbon monoxide at high northern latitudes since 1950 based on measurements on NEEM firn air and the use of the LGGE-GIPSA models of gas transport in firn. Combined with the CO reconstruction from different measurement sets on the same firn air (Petrenko et al., 2011) and an isotope mass balance model, we calculate the temporal evolution of CO source partitioning since 1950. The mass balance model results suggest that variations in fossil-fuel-derived CO are the primary factor behind the observed CO concentration and its $\delta^{18}O$ trends at high northern latitude since 1950. The decrease of CO emission from fossil fuel combustion since the mid-1970s is ascribed to the invention and application of catalytic converters in the Northern Hemisphere, and the growth of diesel engine vehicle market share in Europe, both of which contributing to reduce CO emissions from vehicles.

ACPD
11, 30627–30663, 2011

Supplementary material related to this article is available online at: http://www.atmos-chem-phys-discuss.net/11/30627/2011/acpd-11-30627-2011-supplement.pdf.

Acknowledgements. We sincerely thank J. F. Lamarque, O. Pechony, and A. Ito for sharing with us the biomass/biofuel burning reconstruction data. NEEM is directed and organized by the Center of Ice and Climate at the Niels Bohr Institute and US NSF, Office of Polar Programs. It is supported by funding agencies and institutions in Belgium (FNRS-CFB and FWO), Canada (NRCan/GSC), China (CAS), Denmark (FIST), France (IPEV, CNRS/INSU, CEA and ANR), Germany (AWI), Iceland (RannIs), Japan (NIPR), Korea (KOPRI), The Netherlands (NWO/ALW), Sweden (VR), Switzerland (SNF), UK (NERC) and the USA (US NSF, Office of Polar Programs). We also thank L. Emmons for useful help on MOZART-4 simulation and NCAR for providing supercomputing environment for MOZART-4 simulation. This work was supported by the National Science Foundation grant OCE0731406, the European Science Foundation (ESF) EURO-CORES Programme EuroCLIMATE (contract ERAS-CT-2003-980409 of the European Commission, DG Research, FP6), Institut National des Sciences de l'Univers (INSU) project ISOTRACE-FP21, and the French ANR NEEM (ANR-O7-VULN-09-001). This work has also received funding from the European Community's Seventh Framework Programme (FP7) in the project PEGASOS (grant agreement 265148).

References

van Aardenne, J. A., Dentener, F. J., Olivier, J. G. J., Goldewijk, C., and Lelieveld, J.: A 1° × 1° resolution data set of historical anthropogenic trace gas emissions for the period 1890–1990, Global Biogeochem. Cy., 15, 909–928, 2001.

Assonov, S. S., Brenninkmeijer, C. A. M., Jöckel, P., Mulvaney, R., Bernard, S., and Chappellaz, J.: Evidence for a CO increase in the SH during the 20th century based on firn air samples from Berkner Island, Antarctica, Atmos. Chem. Phys., 7, 295–308, doi:10.5194/acp-7-295-2007, 2007.

Bauer, K., Conrad, R., and Seiler, W.: Photo-oxidative production of carbon monoxide by phototropic mocroorganisms, Biochim. Biophys. Acta, 589, 46–55, 1980.

ACPD

11, 30627–30663, 2011

Bergamaschi, P., Hein, R., Brenninkmeijer, C. A. M., and Crutzen, P. J.: Inverse modeling of the global CO cycle 2. Inversion of $^{13}C/^{12}C$ and $^{18}O/^{16}O$ isotope ratios, J. Geophys. Res.-Atmos., 105, 1929–1945, 2000a.

Bergamaschi, P., Hein, R., Heimann, M., and Crutzen, P. J.: Inverse modeling of the global CO cycle 1. Inversion of CO mixing ratios, J. Geophys. Res.-Atmos., 105, 1909–1927, 2000b.

Bousquet, P., Hauglustaine, D. A., Peylin, P., Carouge, C., and Ciais, P.: Two decades of OH variability as inferred by an inversion of atmospheric transport and chemistry of methyl chloroform, Atmos. Chem. Phys., 5, 2635–2656, doi:10.5194/acp-5-2635-2005, 2005.

Brenninkmeijer, C. A. M.: Measurement of the abundance of ^{14}CO in the atmosphere and the $^{13}C/^{12}C$ and $^{18}O/^{16}O$ ratio of atmospheric CO with applications in New Zealand and Antarctica, J. Geophys. Res.-Atmos., 98, 10595–10614, 1993.

Brenninkmeijer, C. A. M. and Rockmann, T.: Principal factors determining the $^{18}O/^{16}O$ ratio of atmospheric CO as derived from observations in the southern hemispheric troposphere and lowermost stratosphere, J. Geophys. Res.-Atmos., 102, 25477–25485, 1997.

Buizert, C., Martinerie, P., Petrenko, V. V., Severinghaus, J. P., Trudinger, C. M., Witrant, E., Rosen, J. L., Orsi, A. J., Rubino, M., Etheridge, D. M., Steele, L. P., Hogan, C., Laube, J. C., Sturges, W. T., Levchenko, V. A., Smith, A. M., Levin, I., Conway, T. J., Dlugokencky, E. J., Lang, P. M., Kawamura, K., Jenk, T. M., White, J. W. C., Sowers, T., Schwander, J., and Blunier, T.: Gas transport in firn: multiple-tracer characterisation and model intercomparison for NEEM, Northern Greenland, Atmos. Chem. Phys. Discuss., 11, 15975–16021, doi:10.5194/acpd-11-15975-2011, 2011.

Clark, I. D., Henderson, L., Chappellaz, J., Fisher, D., Koerner, R., Worthy, D. E. J., Kotzer, T., Norman, A. L., and Barnola, J. M.: CO_2 isotopes as tracers of firn air diffusion and age in an Arctic ice cap with summer melting, Devon Island, Canada, J. Geophys. Res.-Atmos., 112, D01301, doi:10.1029/2006jd007471, 2007.

Conrad, R. and Seiler, W.: Photooxidative production and microbial consumption of carbon monoxide in seawater, Fems Microbiol. Lett., 9, 61–64, 1980.

Duncan, B. N., Logan, J. A., Bey, I., Megretskaia, I. A., Yantosca, R. M., Novelli, P. C., Jones, N. B., and Rinsland, C. P.: Global budget of CO, 1988–1997: source estimates and validation with a global model, J. Geophys. Res.-Atmos., 112, D22301, doi:10.1029/2007jd008459, 2007.

Emmons, L. K., Walters, S., Hess, P. G., Lamarque, J.-F., Pfister, G. G., Fillmore, D., Granier, C., Guenther, A., Kinnison, D., Laepple, T., Orlando, J., Tie, X., Tyndall, G., Wiedinmyer, C.,

ACPD
11, 30627–30663, 2011

Baughcum, S. L., and Kloster, S.: Description and evaluation of the Model for Ozone and Related chemical Tracers, version 4 (MOZART-4), Geosci. Model Dev., 3, 43–67, doi:10.5194/gmd-3-43-2010, 2010.

EPA: National air pollutant emission trends: 1900–1998, EPA Report 454/R-00-002, United States Environmental Protection Agency, Research Triangle Park, NC 27711, 2000.

Fernandes, S. D., Trautmann, N. M., Streets, D. G., Roden, C. A., and Bond, T. C.: Global biofuel use, 1850–2000, Global Biogeochem. Cy., 21, Gb2019, doi:10.1029/2006gb002836, 2007.

Ferretti, D. F., Miller, J. B., White, J. W. C., Etheridge, D. M., Lassey, K. R., Lowe, D. C., Macfarling Meure, C. M. M., Dreier, M. F., Trudinger, C. M., van Ommen, T. D., and Langenfelds, R. L.: Unexpected changes to the global methane budget over the past 2000 years, Science, 309, 1714–1717, doi:10.1126/science.1115193, 2005.

Haan, D. and Raynaud, D.: Ice core record of CO variations during the last two millennia: atmospheric implications and chemical interactions within the Greenland ice, Tellus B, 50, 253–262, 1998.

Haan, D., Martinerie, P., and Raynaud, D.: Ice core data of atmospheric carbon monoxide over Antarctica and Greenland during the last 200 years, Geophys. Res. Lett., 23, 2235–2238, 1996.

Heidt, L. E., Krasnec, J. P., Lueb, R. A., Pollock, W. H., Henry, B. E., and Crutzen, P. J.: Latitudinal distributions of CO and CH_4 over the Pacific, J. Geophys. Res.-Oc. Atm., 85, 7329–7336, 1980.

Iannone, R., Anderson, R. S., Rudolph, J., Huang, L., and Ernst, D.: The carbon kinetic isotope effects of ozone-alkene reactions in the gas-phase and the impact of ozone reactions on the stable carbon isotope ratios of alkenes in the atmosphere, Geophys. Res. Lett., 30, 1684, doi:10.1029/2003gl017221, 2003.

Iannone, R., Koppmann, R., and Rudolph, J.: $^{12}C/^{13}C$ kinetic isotope effects of the gas-phase reactions of isoprene, methacrolein, and methyl vinyl ketone with OH radicals, Atmos. Environ., 43, 3103–3110, doi:10.1016/j.atmosenv.2009.03.006, 2009.

Ito, A. and Penner, J. E.: Historical emissions of carbonaceous aerosols from biomass and fossil fuel burning for the period 1870–2000, Global Biogeochem. Cy., 19, Gb2028, doi:10.1029/2004gb002374, 2005.

Kato, S., Akimoto, H., Rockmann, T., Braunlich, M., and Brenninkmeijer, C. A. M.: Stable isotopic compositions of carbon monoxide from biomass burning experiments, Atmos. Environ.,

ACPD
11, 30627–30663, 2011

33, 4357–4362, 1999.
Khalil, M. A. K. and Rasmussen, R. A.: Carbon monoxide in the earth's atmosphere: increased trend, Science, 224, 54–56, 1984.
Khalil, M. A. K. and Rasmussen, R. A.: Global decrease in atmospheric carbon monoxide concentration, Nature, 370, 639–641, 1994.
Kummer, J. T.: Catalysis for automobile emission control, Prog. Energ. Combust., 6, 177–199, 1980.
Lamarque, J.-F., Bond, T. C., Eyring, V., Granier, C., Heil, A., Klimont, Z., Lee, D., Liousse, C., Mieville, A., Owen, B., Schultz, M. G., Shindell, D., Smith, S. J., Stehfest, E., Van Aardenne, J., Cooper, O. R., Kainuma, M., Mahowald, N., McConnell, J. R., Naik, V., Riahi, K., and van Vuuren, D. P.: Historical (1850–2000) gridded anthropogenic and biomass burning emissions of reactive gases and aerosols: methodology and application, Atmos. Chem. Phys., 10, 7017–7039, doi:10.5194/acp-10-7017-2010, 2010.
Lean, J., Beer, J., and Bradley, R.: Reconstruction of solar irradiance since 1610 – implications for climate change, Geophys. Res. Lett., 22, 3195–3198, 1995.
Levy, H.: Normal atmosphere – large radical and formaldehyde concentrations predicted, Science, 173, 141–143, 1971.
Logan, J. A., Prather, M. J., Wofsy, S. C., and McElroy, M. B.: Tropospheric chemistry: a global perspective, J. Geophys. Res.-Oc. Atm., 86, 7210–7254, 1981.
Mak, J. E. and Brenninkmeijer, C. A. M.: Measurement of ^{13}CO and $C^{18}O$ in the free troposphere, J. Geophys. Res.-Atmos., 103, 19347–19358, 1998.
Mak, J. E. and Kra, G.: The isotopic composition of carbon monoxide at Montauk Point, Long Island, Chemosphere, 1(1), 205–218, 1999.
Mak, J., Kra, G., Sandomenico, T., and Bergamaschi, P.: The seasonally varying isotopic composition of the sources of carbon monoxide at Barbados, West Indies, J. Geophys. Res.-Atmos., 108, 4635, doi:10.1029/2003jd003419, 2003.
Manning, M. R., Brenninkmeijer, C. A. M., and Allan, W.: Atmospheric carbon monoxide budget of the Southern Hemisphere: implications of $^{13}C/^{12}C$ measurements, J. Geophys. Res.-Atmos., 102, 10673–10682, 1997.
Marland, G., Boden, T. A., and Andres, R. J.: Global, regional, and national fossil-fuel CO_2 emissions, in: Trends: A Compendium of Data on Global Change, Carbon Dioxide Information Analysis Center, Oak Ridge National Laboratory, US Department of Energy, Oak Ridge, TN, USA, 2008.

ACPD
11, 30627–30663, 2011

McConnell, J. R. and Edwards, R.: Coal burning leaves toxic heavy metal legacy in the Arctic, P. Natl. Acad. Sci. USA, 105, 12140–12144, doi:10.1073/pnas.0803564105, 2008.
McConnell, J. R., Lamorey, G. W., and Hutterli, M. A.: A 250-year high-resolution record of Pb flux and crustal enrichment in Central Greenland, Geophys. Res. Lett., 29, 2130, doi:10.1029/2002gl016016, 2002.
Montzka, S. A., Krol, M., Dlugokencky, E., Hall, B., Jockel, P., and Lelieveld, J.: Small interannual variability of global atmospheric hydroxyl, Science, 331, 67–69, doi:10.1126/science.1197640, 2011.
Novelli, P. and Masarie, K. A.: Atmospheric Carbon Monoxide Dry Air Mole Fractions from the NOAA ESRL Carbon Cycle Cooperative Global Air Sampling Network, 1988–2009, Version: 2010-07-14, Path: ftp://ftp.cmdl.noaa.gov/ccg/co/flask/event/ (last access: November 2011), 2010.
Novelli, P. C., Steele, L. P., and Tans, P. P.: Mixing ratios of carbon monoxide in the troposphere, J. Geophys. Res.-Atmos., 97, 20731–20750, 1992.
Novelli, P. C., Masarie, K. A., Tans, P. P., and Lang, P. M.: Recent changes in atmospheric carbon monoxide, Science, 263, 1587–1590, 1994.
Park, K.: Joint Application of Concentration and Isotope Ratios to Investigate the Global Atmospheric Carbon Monoxide Budget: An Inverse Modeling Approach, PhD Thesis, Stony Brook University, Stony Brook, NY, USA, 2010.
Pechony, O. and Shindell, D. T.: Driving forces of global wildfires over the past millennium and the forthcoming century, P. Natl. Acad. Sci. USA, 107, 19167–19170, doi:10.1073/pnas.1003669107, 2010.
Petrenko, V., Martinerie, P., Novelli, P., Etheridge, D. M., Levin, I., Wang, Z., Petron, G., Blunier, T., Chappellaz, J., Kaiser, J., Lang, P., Steele, L. P., Vogel, F., Leist, M. A., Mak, J., Langenfelds, R. L., Schwander, J., Severinghaus, J. P., Forster, G., Sturges, W., Rubino, M., and White, J. W. C.: Records of Northern Hemisphere carbon monoxide and hydrogen back to ∼ 1950 from Greenland firn air, Atmos. Chem. Phys., in preparation, 2011.
Petron, G., Granier, C., Khattatov, B., Yudin, V., Lamarque, J. F., Emmons, L., Gille, J., and Edwards, D. P.: Monthly CO surface sources inventory based on the 2000–2001 MOPITT satellite data, Geophys. Res. Lett., 31, L21107, doi:10.1029/2004gl020560, 2004.
Pongratz, J., Reick, C., Raddatz, T., and Claussen, M.: A reconstruction of global agricultural areas and land cover for the last millennium, Global Biogeochem. Cy., 22, GB3018, doi:10.1029/2007gb003153, 2008.

ACPD
11, 30627–30663, 2011

Prinn, R. G., Huang, J., Weiss, R. F., Cunnold, D. M., Fraser, P. J., Simmonds, P. G., McCulloch, A., Harth, C., Reimann, S., Salameh, P., O'Doherty, S., Wang, R. H. J., Porter, L. W., Miller, B. R., and Krummel, P. B.: Evidence for variability of atmospheric hydroxyl radicals over the past quarter century, Geophys. Res. Lett., 32, L07809, doi:10.1029/2004gl022228, 2005.

Rinsland, C. P. and Levine, J. S.: Free tropspheric carbon monoxide concentrations in 1950 and 1951 deduced from infrared total column amount measurements, Nature, 318, 250–254, 1985.

Röckmann, T., Jöckel, P., Gros, V., Bräunlich, M., Possnert, G., and Brenninkmeijer, C. A. M.: Using ^{14}C, ^{13}C, ^{18}O and ^{17}O isotopic variations to provide insights into the high northern latitude surface CO inventory, Atmos. Chem. Phys., 2, 147–159, doi:10.5194/acp-2-147-2002, 2002.

Rommelaere, V., Arnaud, L., and Barnola, J. M.: Reconstructing recent atmospheric trace gas concentrations from polar firn and bubbly ice data by inverse methods, J. Geophys. Res.-Atmos., 102, 30069–30083, 1997.

Rudolph, J., Lowe, D. C., Martin, R. J., and Clarkson, T. S.: A novel method for compound specific determination of $\delta^{13}C$ in volatile organic compounds at ppt levels in ambient air, Geophys. Res. Lett., 24, 659–662, 1997.

Rudolph, J., Czuba, E., and Huang, L.: The stable carbon isotope fractionation for reactions of selected hydrocarbons with OH-radicals and its relevance for atmospheric chemistry, J. Geophys. Res.-Atmos., 105, 29329–29346, 2000.

Schwander, J. and Stauffer, B.: Age difference between polar ice and the air trapped in its bubbles, Nature, 311, 45–47, 1984.

Seiler, W.: Cycle of atmospheric CO, Tellus, 26, 116–135, 1974.

Seiler, W. and Junge, C.: Carbon monoxide in atmosphere, J. Geophys. Res., 75, 2217–2226, 1970.

Stevens, C. M. and Wagner, A. F.: The role of isotope fractionation effects in atmospheric chemistry, Z. Naturfosch. A, 44, 376–384, 1989.

Stevens, C. M., Walling, D., Venters, A., Ross, L. E., Engelkem, A., and Krout, L.: Isotopic composition of atmospheric carbon-monoxide, Earth Planet. Sc. Lett., 16, 147–165, 1972.

Tarr, M. A., Miller, W. L., and Zepp, R. G.: Direct carbon monoxide photoproduction from plant matter, J. Geophys. Res.-Atmos., 100, 11403–11413, 1995.

Tsunogai, U., Hachisu, Y., Komatsu, D. D., Nakagawa, F., Gamo, T., and Akiyama, K.: An

ACPD
11, 30627–30663, 2011

updated estimation of the stable carbon and oxygen isotopic compositions of automobile CO emissions, Atmos. Environ., 37, 4901–4910, doi:10.1016/j.atmosenv.2003.08.008, 2003.
Wang, Z. and Mak, J. E.: A new CF-IRMS system for quantifying stable isotopes of carbon monoxide from ice cores and small air samples, Atmos. Meas. Tech., 3, 1307–1317, doi:10.5194/amt-3-1307-2010, 2010.
Wang, Z., Chappellaz, J., Park, K., and Mak, J. E.: Large variations in Southern Hemisphere biomass burning during the last 650 years, Science, 330, 1663–1666, doi:10.1126/science.1197257, 2010.
Wang, Z., Park, K., and Mak, J. E.: Interannual variations of anthropogenic source of atmospheric CO at high northern latitudes during 2004–2009, in preparation, 2011.
Weinstock, B.: Carbon monoxide: residence time in atmosphere, Science, 166, 224–225, 1969.
van der Werf, G. R., Randerson, J. T., Giglio, L., Collatz, G. J., Kasibhatla, P. S., and Arellano Jr., A. F.: Interannual variability in global biomass burning emissions from 1997 to 2004, Atmos. Chem. Phys., 6, 3423–3441, doi:10.5194/acp-6-3423-2006, 2006.
Witrant, E., Martinerie, P., Hogan, C., Laube, J. C., Kawamura, K., Capron, E., Montzka, S. A., Dlugokencky, E. J., Etheridge, D., Blunier, T., and Sturges, W. T.: A new multi-gas constrained model of trace gas non-homogeneous transport in firn: evaluation and behavior at eleven polar sites, Atmos. Chem. Phys. Discuss., 11, 23029–23080, doi:10.5194/acpd-11-23029-2011, 2011.
Young, L. C. and Finlayson, B. A.: Mathematical models of monolith catallytic converter 2: application to automobile exhaust, Aiche J., 22, 343–353, 1976.

ACPD
11, 30627–30663, 2011

Table 1. MOZART-4 simulations on atmospheric CO at Iceland in January 1997–December 2004.

Sources	$[CO]_{source}$	Relative contribution	Source $\delta^{18}O$ (‰)[a]	$\delta^{18}O$ at Iceland (‰)[b]
Fossil fuel	40	32 %	24	20
Methane oxidation	28	22 %	0	−9
NMHC oxidation	21	17 %	0	−8
Biofuel	12	10 %	18	10
Biomass burning	12	9 %	18	9
Biogenic	11	9 %	0	−5
Ocean	1	1 %	15	10

[a] These are original $\delta^{18}O$ signatures used for each type of emission in the model.
[b] $\delta^{18}O$ at Iceland is the isotopic ratio calculated in the model based on the ratio between $[C^{16}O]$ and $[C^{18}O]$ at Iceland. Data after Park (2010).

ACPD
11, 30627–30663, 2011

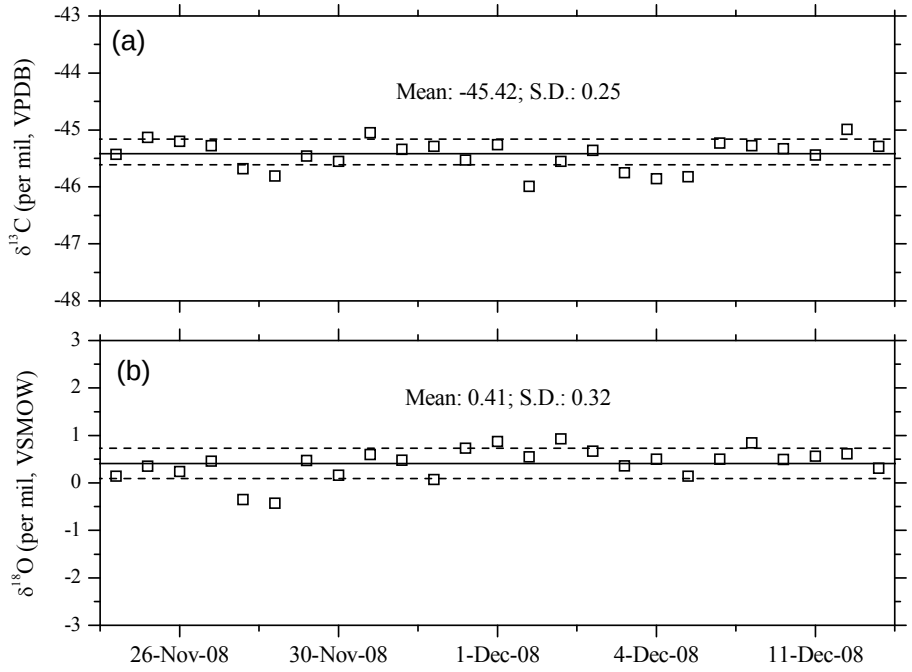

Fig. 1. Measurements of **(a)** δ^{13}C and **(b)** δ^{18}O(CO_2) for calibration gas during the measurement period of the NEEM firn air samples (see details of method in Wang and Mak, 2010). S.D. stands for $\pm 1\sigma$ standard deviation.

ACPD
11, 30627–30663, 2011

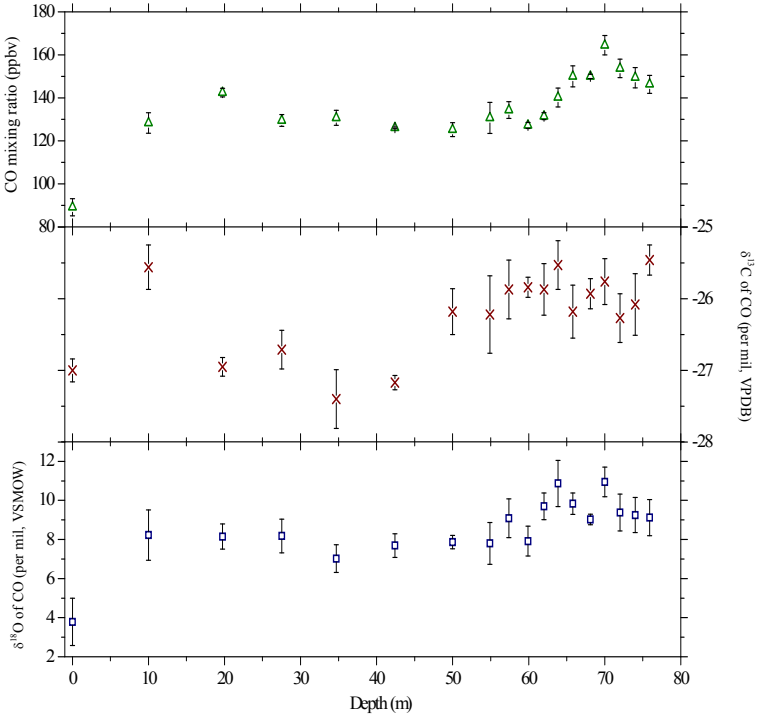

Fig. 2. Observations for the mixing ratio and isotopic ratios of CO in NEEM firn air collected from the EU 2008 borehole. Top panel: [CO] in this study (green squares); middle panel: δ^{13}C of CO in this study (cross); bottom: δ^{18}O of CO in this study. Error bars are $\pm 1\sigma$ standard deviations on replicates from 3 to 12 measurements at each depth level.

ACPD
11, 30627–30663, 2011

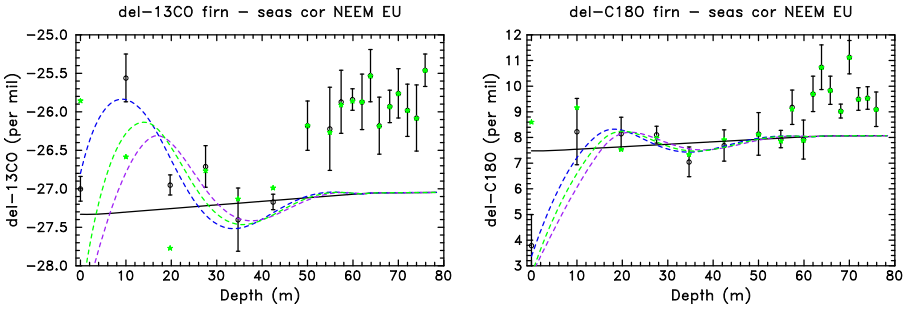

Fig. 3. Estimation of the effect of atmospheric seasonality on δ^{13}C (left) and δ^{18}O (right) of CO in NEEM firn. Measured isotopic ratios are shown as black circles with error bars, and green stars show δ^{13}C and δ^{18}O values corrected from the effect of seasonality. Simulated values with constant atmospheric trends are plotted as black lines, simulated values with constant atmospheric trends and perpertual mean seasonal cycle are plotted as green dashed lines. The increasing isotopic ratios with depth obtained from constant scenarios (black lines) illustrate the effect of gravitational fractionation. The purple and blue dashed lines illustrate the effect of shifting the final date of the simulation (drill date) by plus or minus 15 days, respectively.

ACPD
11, 30627–30663, 2011

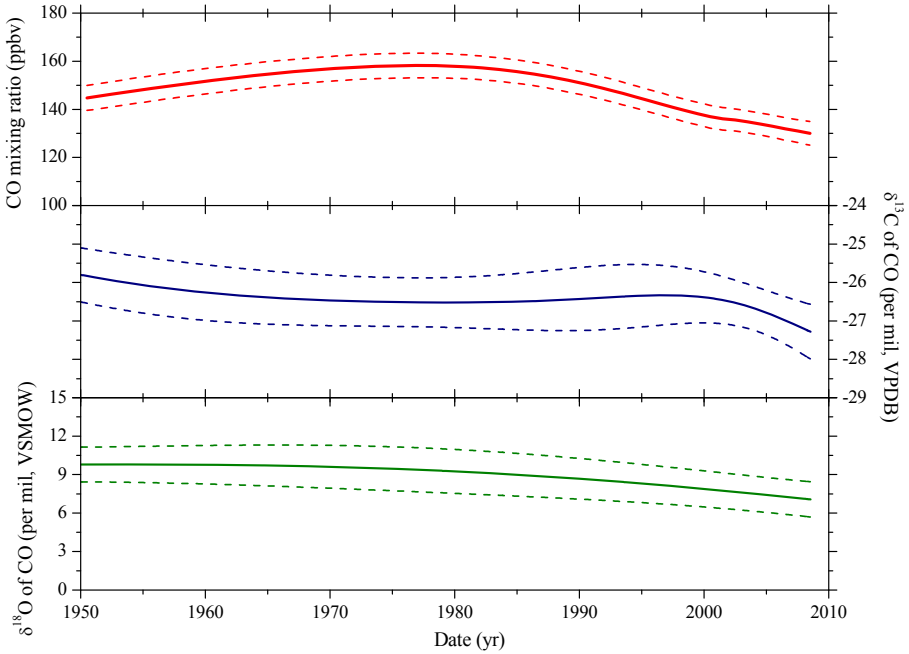

Fig. 4. Best estimate trends of CO concentration (Petrenko et al., 2011) and isotopic ratios simulated by LGGE-GIPSA models of gas transport in firn. Best estimate time trends and uncertainty envelopes in firn are shown as continuous black lines and dashed black lines, respectively.

ACPD
11, 30627–30663, 2011

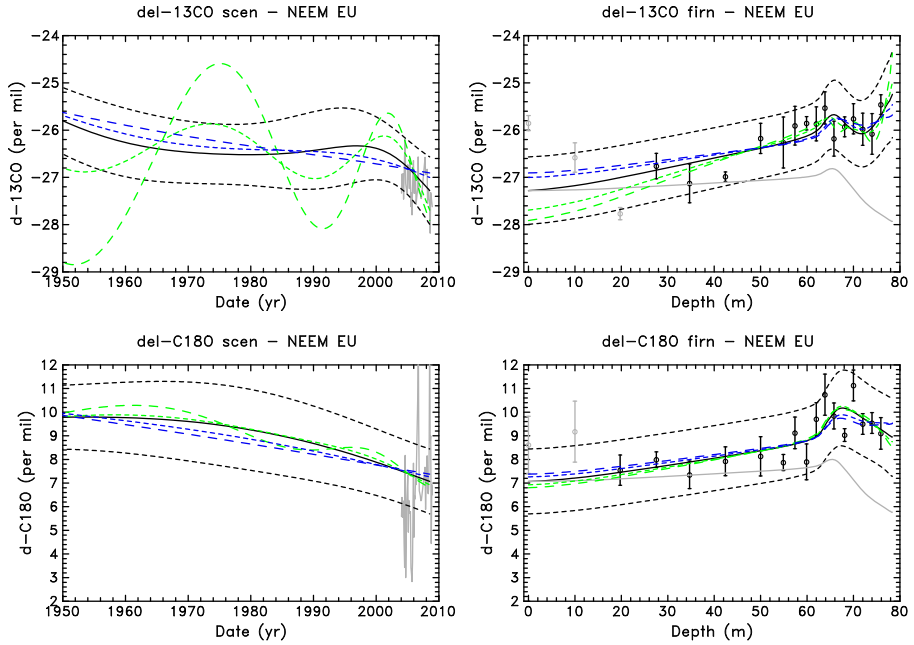

Fig. 5. Best estimate trends of CO isotopes and influence of the regularization factor. Best estimate time trends (in black) and the resulting isotopic ratios in firn are the same as in Fig. 4. The grey lines on right panels show the effect of the CO trend scenario with constant atmospheric isotopic ratio. Blue lines show the effect of increasing the weight of the regularization term by a factor of 10 (short dashed lines) and 100 (long dashed lines). Green lines show the effect of decreasing the weight of the regularization term by a factor of 10 (short dashed lines) and 100 (long dashed lines). The circles with error bars on right panels show the measurements, and those in grey were not used in the scenario reconstruction. Grey lines on the right panels show the de-seasonalized atmospheric trends in Iceland (Wang et al., 2011).

ACPD
11, 30627–30663, 2011

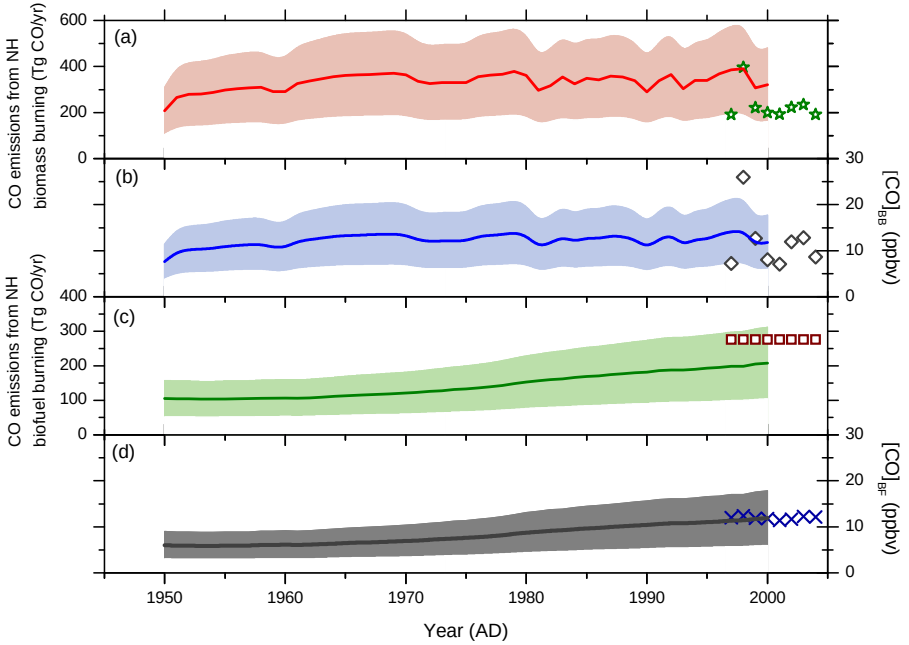

Fig. 6. (a) and **(c)**: estimated CO emissions from NH biomass and biofuel burning (Tg CO yr^{-1}) based on model simulation (Ito and Penner, 2005). Also shown are 1997–2004 NH CO emission inventory of biomass burning (van der Werf et al., 2006) (green stars) and biofuel burning (Petron et al., 2004) (red squares), used in MOZART-4 simulation (Park, 2010). **(b)** and **(d)**: calculated CO contribution (ppbv) from biomass ($[CO]_{BB}$) and biofuel ($[CO]_{BF}$ burning by scaling (see text), which is used in the isotope mass balance model. Also shown are CO contributions from biomass burning (grey diamonds) and biofuel burning (blue crosses) at high northern latitudes in MOZART-4 simulation (Park, 2010). Shading areas show the ± 50 % uncertainty for estimating both biomass burning and biofuel burning emissions.

ACPD
11, 30627–30663, 2011

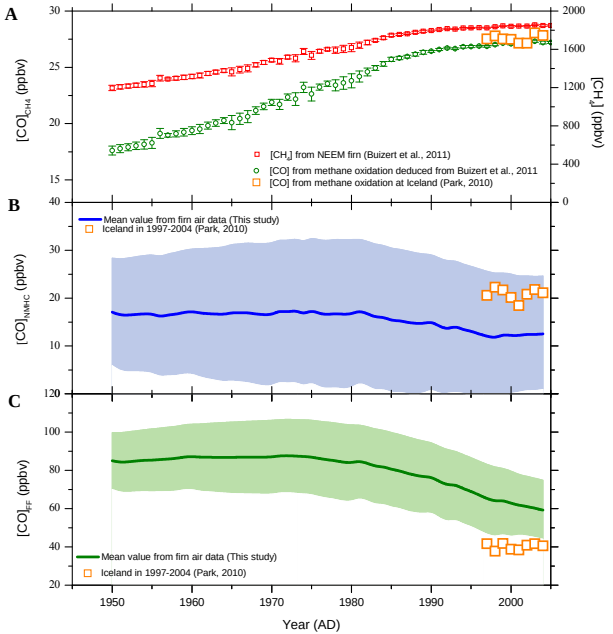

Fig. 7. Modeled CO source partitioning based on observations and isotope mass balance model: **(A)** Methane atmospheric trend at high northern latitude (Buizert et al., 2011) (red squares) and [CO] from methane oxidation ($[CO]_{CH_4}$) deduced from the methane concentration (green circles); **(B)** [CO] from NMHC oxidation ($[CO]_{NMHC}$), and **(C)** [CO] from fossil fuel combustion ($[CO]_{FF}$). Thick lines in **(B)** and **(C)** represent the mean values of different scenarios and shaded areas represent the uncertainties which arise from the LGGE-GIPSA models simulation uncertainties on both CO concentration and $\delta^{18}O$ as well as the uncertainties for estimating historical CO emissions from biofuel and biomass burning (Ito and Penner, 2005). [CO] derived from the three major sources since 1950 is calculated based on an isotope mass balance model (Wang et al., 2010). CO source partitioning at present day is calculated based on MOZART-4 simulation and CO measurements in 1997–2004 at Iceland (orange squares) (Park, 2010).

ACPD
11, 30627–30663, 2011

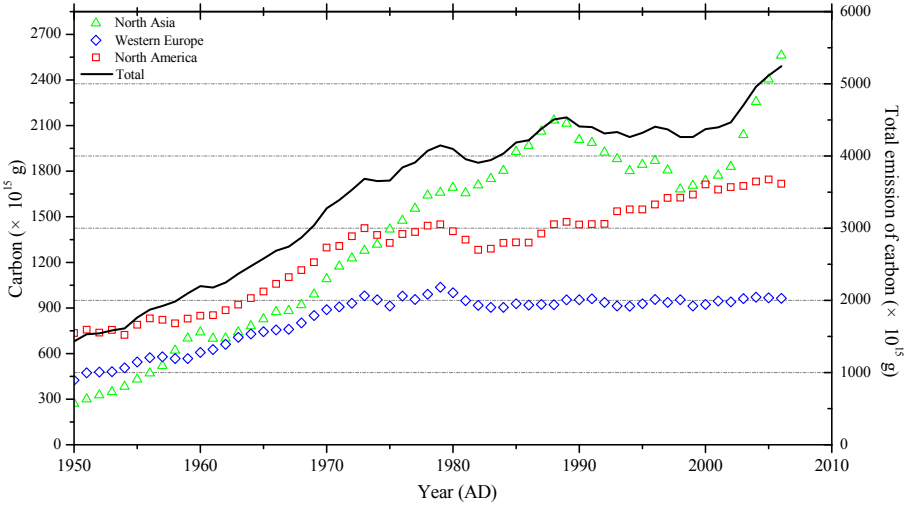

Fig. 8. Fossil-Fuel CO_2 emissions in these mid-high latitude Northern Hemisphere regions. Symbols link to left y-axis and indicate the CO_2 emissions in three different regions: green triangles: North Asia; blue diamonds: Western Europe; red squares: North America. Black line links to right y-axis and stands for the sum of CO_2 emissions from the above three regions (Marland et al., 2008).

ACPD
11, 30627–30663, 2011

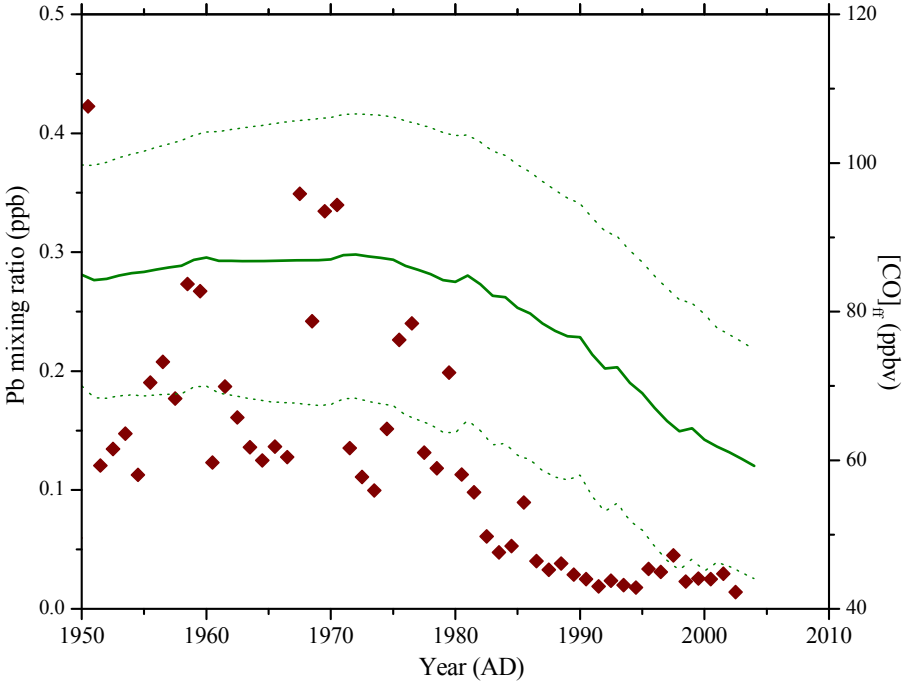

Fig. 9. Correlation between Greenland lead concentrations in snow cores (McConnell and Edwards, 2008) and our reconstructed CO contribution from fossil fuel combustion in 1950–2000 (same as Fig. 7c: solid line shows the mean values and dotted lines show the uncertainties).

ACPD
11, 30627–30663, 2011